The role of electron heat flux in guide-field magnetic reconnection

Michael Hesse, Masha Kuznetsova, and Joachim Birn

Citation: Physics of Plasmas (1994-present) **11**, 5387 (2004); doi: 10.1063/1.1795991
View online: http://dx.doi.org/10.1063/1.1795991
View Table of Contents: http://scitation.aip.org/content/aip/journal/pop/11/12?ver=pdfcov
Published by the AIP Publishing

The role of electron heat flux in guide-field magnetic reconnection

Michael Hesse and Masha Kuznetsova
NASA Goddard Space Flight Center, Greenbelt, Maryland 20771

Joachim Birn
Los Alamos National Laboratory, Los Alamos, New Mexico 87545

(Received 20 April 2004; accepted 23 July 2004; published online 29 October 2004)

A combination of analytical theory and particle-in-cell simulations are employed in order to investigate the electron dynamics near and at the site of guide field magnetic reconnection. A detailed analysis of the contributions to the reconnection electric field shows that both bulk inertia and pressure-based quasiviscous processes are important for the electrons. Analytic scaling demonstrates that conventional approximations for the electron pressure tensor behavior in the dissipation region fail, and that heat flux contributions need to be accounted for. Based on the evolution equation of the heat flux three tensor, which is derived in this paper, an approximate form of the relevant heat flux contributions to the pressure tensor is developed, which reproduces the numerical modeling result reasonably well. Based on this approximation, it is possible to develop a scaling of the electron current layer in the central dissipation region. It is shown that the pressure tensor contributions become important at the scale length defined by the electron Larmor radius in the guide magnetic field. © *2004 American Institute of Physics*. [DOI: 10.1063/1.1795991]

I. INTRODUCTION

Magnetic reconnection is a process, which facilitates plasma transport across magnetic field lines and magnetic topologies[1] in a system, where plasma ions and electrons are tied to magnetic flux tubes almost everywhere in the volume under consideration.[2] The disconnection and reconnection of plasma elements is accomplished by processes that generate, in a localized region in space, deviations from the frozen-in condition, or ideal Ohm's law:

$$\mathbf{E} + \mathbf{v}_s \times \mathbf{B} = 0. \tag{1}$$

Here $\mathbf{E}$ and $\mathbf{B}$ denote electric and magnetic fields, and $\mathbf{v}_s$ the velocity of particle species s. In order for reconnection to proceed, Eq. (1) needs to be violated by all particle species involved individually. Since it is physically clear that violating Eq. (1) is most difficult for electrons, we will, in this paper, concentrate on the behavior of electrons.

Under this premise, the electron momentum equation can, in the absence of classical collisions, be derived from the Vlasov equations. In the electron rest frame, one obtains without further approximations[3]

$$\mathbf{E} = -\mathbf{v}_e \times \mathbf{B} - \frac{1}{n_e e} \nabla \cdot \overleftrightarrow{\mathbf{P}}_e - \frac{m_e}{e}\left(\frac{\partial \mathbf{v}_e}{\partial t} + \mathbf{v}_e \cdot \nabla \mathbf{v}_e\right). \tag{2}$$

As evident from Eq. (2), the macroscopic manifestations of magnetic reconnection have to be related to thermal inertia terms (the divergence of the electron pressure tensor), or bulk inertia terms with temporal or spatial derivatives of the electron bulk flow speed.

This electron dynamics in collisionless magnetic reconnection has been the subject of a number of recent studies, most of which are based on particle-in-cell simulations.[4–14] While addressing only a limited spatial system, and limited by physical parameters such as the ion-electron mass ratio, particle-in-cell simulations permit a self-consistent connection between the electromagnetic field evolution and the orbits of charge carriers.

As a result of these simulations, as well as of analytical arguments,[1,15,16] a picture emerged where the pressure related term in Eq. (2) plays the dominant role in the reconnection of antiparallel, or nearly antiparallel magnetic fields. Specifically, the reconnection electric field is, in excellent approximation, described by

$$E_y = -\frac{1}{n_e e}\left(\frac{\partial P_{xy}}{\partial x} + \frac{\partial P_{yz}}{\partial z}\right). \tag{3}$$

Here we have, without loss of generality, assumed that the reconnecting magnetic fields lie in the (poloidal) x-z plane. The generation of nongyrotropic tensor elements in Eq. (3) has been explained by the bounce motion of electrons in the field reversal region,[17] and quantified by a combination of analytical arguments and targeted numerical modeling.[7,18]

In the presence of a guide magnetic field along the current direction, however, the mechanism may, in principle, change. Indeed, Pritchett and Coroniti[19] argued, based on three-dimensional particle-in-cell modeling that guide field reconnection relies primarily on electron bulk inertia. Once the guide field magnitude exceeds a threshold, the Lorentz force associated with it will distort and ultimately eliminate the electron bounce motion in the poloidal field reversal region and pressure-based dissipation may be suppressed. Notionally, this transition has to take place once the electron Larmor radius in the guide magnetic field becomes comparable to the inner gradient scale length of the reconnecting magnetic field. The electron bounce width in the reconnecting magnetic field component B_x is given by[20]

$$\lambda_z = \left[\frac{2m_e T_e}{e^2 B_x'^2} \right]^{1/4}, \tag{4}$$

where B_x' denotes the derivative of B_x with respect to the direction normal to the current sheet (z). Electron orbits become strongly modified once the thermal electron Larmor radius $r_L = v_{the}/\Omega_e$ equals the bounce width (4). After a small amount of algebra, one finds that this condition is equivalent to

$$B_y = B_x' \lambda_z. \tag{5}$$

Equation (5) states that electron bounce orbits in the field reversal region become affected by the presence of a finite guide magnetic field once the magnitude of the latter is as big as that of the reconnecting magnetic field at location of the farthest excursion of an electron bounce motion.

In this paper, we will investigate a system, where B_y exceeds the threshold (5). While a number of studies have addressed magnetic reconnection in the presence of a guide field in both two- and three-dimensional models,[10,19,21,22] one recent analysis indicated that electron nongyrotropies may play a significant role here also,[8] and a recent three-dimensional modeling result supports an alternative, inertia-based dissipation process.[19] Thus, further analyses are required to study in more detail the relative importance of thermal vs bulk inertial effects, and to understand the generation mechanism of any nongyrotropies which may be present in the calculation. This is the purpose of the present investigation.

This paper is organized as follows: Section II contains a brief introduction of the modeled system and of the simulation code applied to the problem. Section III discusses features of the overall system evolution and presents an analysis of the immediate inner reconnection region. Section IV focuses on the primary question of this paper—the dominant dissipation mechanism. Section V extends this analysis to include studies of electron distribution functions and approximate forms of the electron pressure tensor are derived in Sec. VI. An approximate form of the heat flux tensor is derived in Sec. VII and Sec. VIII focuses on scaling laws for component magnetic reconnection. Finally, Sec. IX presents a summary and conclusions.

II. THE MODEL AND MODELED CONFIGURATION

During the discussion, we will employ dimensionless quantities. For this purpose, we normalize densities by a typical density n_0 in the current sheet, the magnetic field by the asymptotic value of the reconnecting magnetic field B_0. Ions are assumed to be protons (mass m_p) throughout, and length scales are normalized by the ion inertial length c/ω_i, where the ion plasma frequency $\omega_i = \sqrt{e^2 n_0/\varepsilon_0 m_p}$ is evaluated for the reference density. Velocities are measured in units of the ion Alfvén velocity $v_A = B_0/\sqrt{\mu_0 m_p n_0}$ based on the reference magnitudes of magnetic field and density. The electric field is measured in units of $E_0 = v_A B_0$, the pressure in units of $p_0 = B_0^2/\mu_0$, and the current density is normalized to $j_0 = \omega_i B_0/c\mu_0$.

The poloidal magnetic field, a modified Harris sheet[23] is of the following form:

$$B_x = \tanh(2z) + a_0 \pi/L_z \cos(2\pi x/L_x)\sin(\pi z/L_z), \tag{6}$$

$$B_z = -a_0 2\pi/L_z \sin(2\pi x/L_x)\cos(\pi z/L_z). \tag{7}$$

The perturbation amplitude $a_0 = 0.1$ leads to an initial value of the normal magnetic field of about 3% of B_0. The system size, $L_x = 25.6$ and $L_z = 12.8$, matches that of the Geospace Environment Modeling Program (GEM) reconnection challenge. Similar to earlier studies,[8] we here employ a constant magnetic field component directed along the main current flow

$$B_y = B_{y0} = 0.8. \tag{8}$$

The ion-electron mass ratio is chosen to be $m_i/m_e = 256$. A total of 1×10^8 macroparticles are employed during the calculation and an electron/ion temperature ratio of $T_e/T_i = 0.2$ has been adopted.

The system evolution is modeled by our particle-in-cell code. Particle orbits are calculated in the electromagnetic fields, and the electromagnetic fields are integrated by an implicit method on a grid composed of 800×800 cells in x and z directions, respectively. Periodic boundary conditions are employed in the x direction, whereas the particles are specularly reflected at the upper and lower boundaries. In order to reduce noise, the code output is averaged over 60 electron plasma periods, centered at the time of interest.

III. EVOLUTION OF THE RECONNECTING SYSTEM

An overview of the evolution, shown in Fig. 1, demonstrates the similarity of the reconnecting system to that found in calculations without guide field components. The initial, X-type perturbation leads to a reconfiguration. The most prominent difference to antiparallel merging is the inclination of the reconnecting current sheet with respect to the x axis. Figure 1 also shows the presence of a very thin current sheet in the central reconnection region, which is likely associated with electron demagnetization.

The panels of Fig. 2 show a blowup of the inner reconnection region, taken at $t = 16$. The top panel shows poloidal magnetic field lines and the total current density, as well as electron flow velocities. The center panel shows that strong electron flows are associated with strong gradients of the magnetic guide-field component B_y. The plot demonstrates the presence of a quadrupolelike magnetic perturbation, albeit strongly distorted, and on top of the underlying guide field magnitude of $B_{y0} = 0.8$. Finally, the lower panel of Fig. 2 displays the electron flow speed in the y direction. While flow velocity magnitudes are of similar magnitude as those found in simulations of antiparallel merging, the layer is strongly concentrated on a scale substantially smaller than the ion inertial length. We point out that the relative drift between ions and electrons in the present calculation is, for the temperatures encountered in the simulation, close to but not larger than the marginally Buneman-unstable threshold.

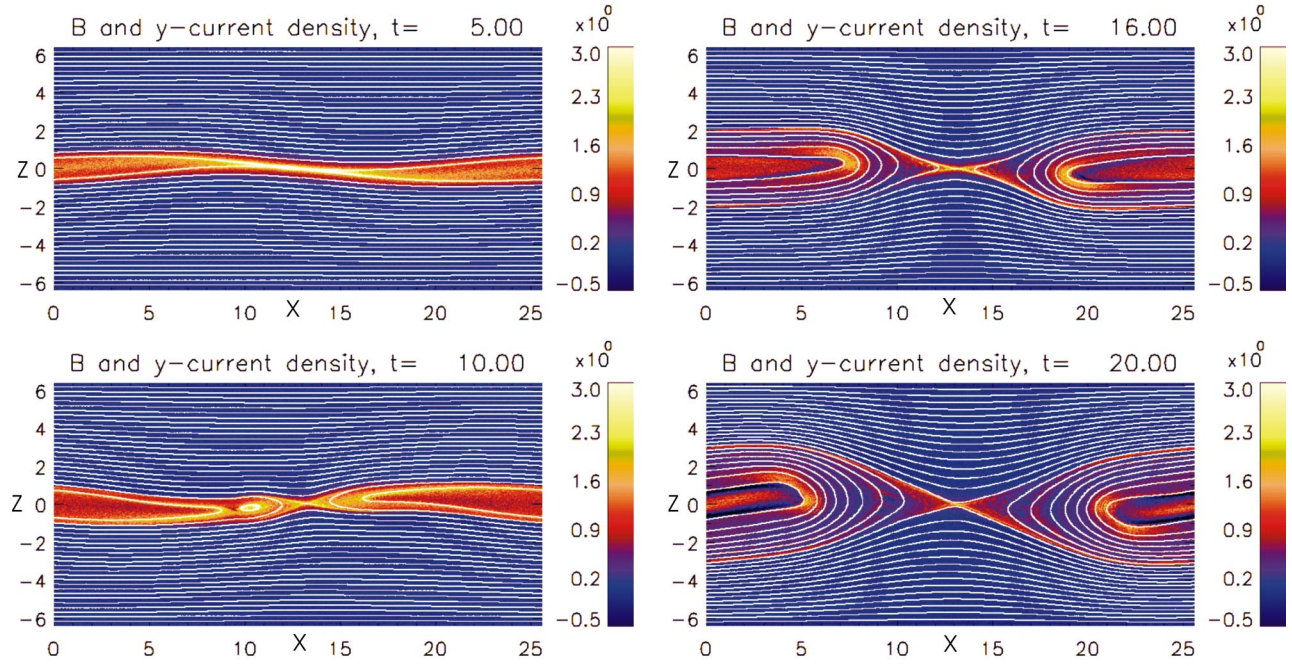

FIG. 1. (Color online). Magnetic field lines and y component of the current density at different simulation times. After a slow phase, the system develops a very thin current sheet in the central diffusion region, which is inclined relative to the x axis.

Figure 3 displays the time evolution of the reconnected magnetic flux, defined as the integral of the normal magnetic field component along the x axis, for simulations with three different values of the guide magnetic field. The graphs indicate a slowdown of the reconnection rate with guide field magnitude. This is particularly apparent for a guide field value of $B_{y0}=0.8$, when compared to the two lower cases. This result indicates that reconnection may favor sites of antiparallel merging over those of component merging, if other conditions are equal.

In the following section, we will analyze the dissipation mechanism, which provides a reconnection electric field in the central region of the diffusion zone.

IV. DISSIPATION: ELECTRON PRESSURE VS BULK INERTIA

Because of the smallness of scale lengths encountered in the preceding section, we extend the electric field equation (3) to include the effects of electron bulk flow inertia. With this inclusion, Eq. (3) becomes

$$E_y = -\frac{1}{n_e e}\left(\frac{\partial P_{xy}}{\partial x}+\frac{\partial P_{yz}}{\partial z}\right)-\frac{m_e}{e}\left(\frac{\partial v_{ey}}{\partial t}+\mathbf{v}_e\cdot\boldsymbol{\nabla} v_{ey}\right). \quad (9)$$

An inspection of Figs. 2 and 3 immediately shows that the first, time-dependent, inertia term cannot contribute significantly to the total reconnection electric field.

The analysis of the remaining terms, together with the electron convection electric field

$$E_{yc} = -(v_{ez}B_x - v_{ex}B_z) \quad (10)$$

is shown in Fig. 4. The top panel shows the total reconnection electric field, the second panel exhibits the electron convection electric field, the third panel displays the inertia contribution, as defined by the last term in Eq. (9), and the bottom panel shows the pressure tensor contribution to the electric field. Clearly, the drop of the convection electric field component near $x=13$ and $z=0$ is a result of the vanishing poloidal magnetic field components. The pressure tensor term, however, contributes substantially to the total electric field, specifically within the region around $x=13$ and $z=0$. Here the pressure tensor derivatives make up the majority of the y component of the electric field, and, accordingly, dominate the reconnection process.

In addition to the pressure tensor contribution, we also find that the inertia term in Eq. (9) provides an appreciable addition to the total electric field. This new role of inertia in the dissipation process is a result of the substantially reduced scale sizes in the reconnection region. With gradient scale lengths of the order of an electron Larmor radius, and smaller than the collisionless skin depth (see below), the inertia term becomes non-negligible at the edges of the strong current channel in the dissipation region.

The main contribution, however, remains due to the electron pressure tensor. In light of the expected electron magnetization in the relatively strong guide field, it might be expected that the expected electron distributions should be largely gyrotropic, yielding a pressure tensor of the form

$$\overleftrightarrow{\mathbf{P}}_{eg} = p_\perp \mathbf{1} + \frac{p_\parallel - p_\perp}{B^2}\vec{B}\vec{B}. \quad (11)$$

However, the electric field contribution due to the gyrotropic electron pressure of the form (11),

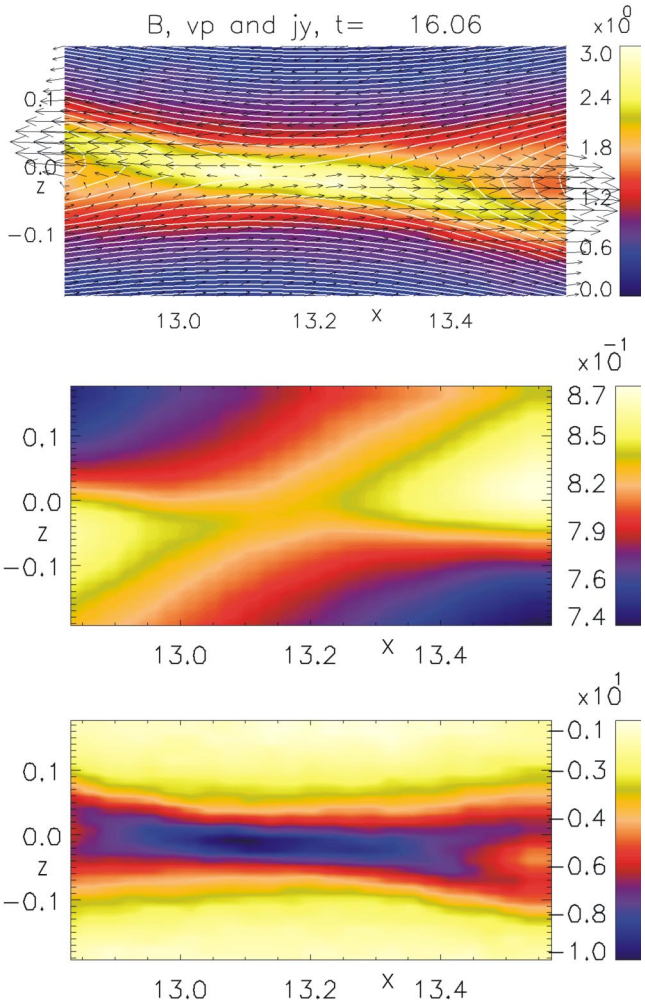

FIG. 2. (Color online). Detailed analysis of the reconnection region at $t=16$. Shown are Poloidal magnetic field, y component of the current density, and poloidal electron flow velocity (top panel); out-of-plane magnetic field B_y and electron flow velocity v_{ey} (center and bottom panels, respectively).

$$-enE_y = \nabla \cdot \vec{\vec{\mathbf{P}}}_{eg}|_y = B_y \vec{B} \cdot \nabla \frac{p_\parallel - p_\perp}{B^2} + \frac{p_\parallel - p_\perp}{B^2} \vec{B} \cdot \nabla B_y, \tag{12}$$

vanishes at the reconnection site, where both B_x and B_z vanish. As a result, deviations from gyrotropy are necessary in order to explain the major component of the reconnection electric field. In the following sections, we will explore the nature of electron distributions, and perform a detailed analysis of the mechanism responsible for electron nongyrotropy.

V. ELECTRON DISTRIBUTIONS

For simplicity we will study in the following reduced distribution functions, defined by, e.g.,

$$F(v_x, v_y) = \int dv_z f(v_x, v_y, v_z).$$

Figures 5 and 6 show reduced electron distribution functions, taken by accumulating particles in the shaded regions. Figure

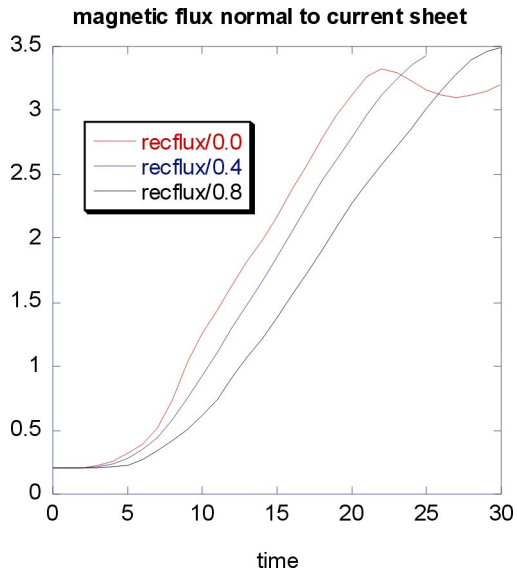

FIG. 3. (Color online). Evolution of the normal magnetic flux for three calculations: With vanishing initial guide field (red), with a 40% guide field (blue), and with an 80% guide field (black). The latter case is the focus of the present paper.

5 shows distribution functions in the central electron dissipation region. While the reduced distribution $F(v_x, v_z)$ appears isotropic (middle panel), the other two distributions feature extended tails in the v_y direction, antiparallel to the current density flow. Thus, in the very center of the current layer, electrons are essentially gyrotropic, with a presence of accelerated electrons along the magnetic field. It should be noted that the distribution should be expected to be gyrotropic only at the central point of the current layer—at any different location the distribution will exhibit nongyrotropies.

Thus, as the observing location is moving away from the central point of the reconnection region, electron distributions rapidly develop nongyrotropies. As an example, Fig. 6 shows reduced electron distributions accumulated a considerable distance away from the reconnection region, in the major outflow channel (see Fig. 2). The distributions show an overall orientation along the local magnetic field with some noticeable deviations (see below). As a result of the poloidal magnetic field, the lower left panel shows an inclination of the distribution in the v_x direction, whereas the lower right panel exhibits a distribution inclined in the v_z direction. The distribution in the center panel, $F(v_x, v_z)$ is not isotropic anymore, indicative of finite electron streaming along the poloidal magnetic field also.

While the distributions of Fig. 5 appear to be essentially gyrotropic, immediately adjacent distributions show evidence of deviations from gyrotropy. As a specific example, the lower left panel of Fig. 6 shows, for higher energies, an apparent small asymmetry relative to the main axis of the distribution, which is given by the local magnetic field direction. According to Eq. (12), such small deviations have to play an important role in the reconnection process. We will, in the following, provide a scaling of the electron pressure tensor evolution, which assumes that the pressure tensor is mostly gyrotropic and develop an approximate, leading-order

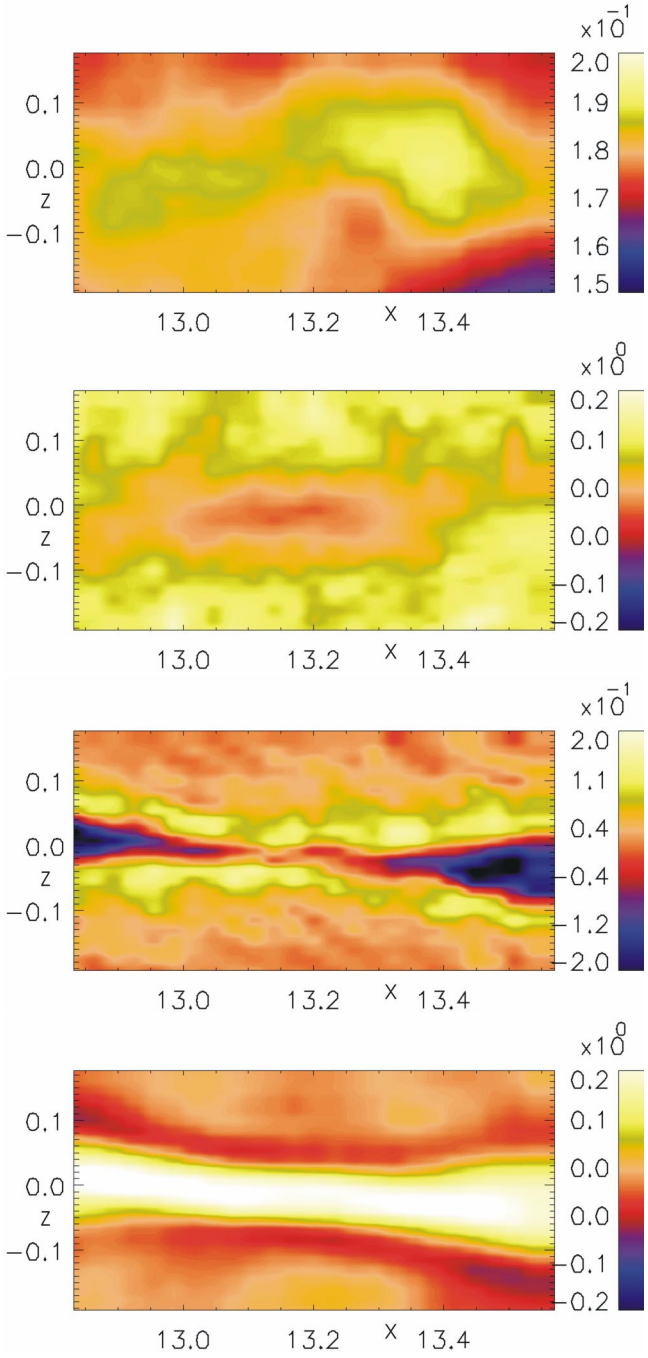

FIG. 4. (Color online). Contributions to the total electric field near the reconnection region for $t=16$. The panels show the total electric field, the electron convection contribution, and electron inertial and quasiviscous, pressure tensor-derived electric fields.

theory for the nongyrotropic components near the central reconnection region.

VI. PRESSURE TENSOR APPROXIMATIONS

Key to understanding the development of nongyrotropic pressures is an analysis of the pressure tensor evolution. In the center-of-mass system of the electron fluid, the electron pressure tensor takes the form[24]

$$\frac{\partial \overleftrightarrow{\mathbf{P}}_e}{\partial t} = -\nabla\cdot(\mathbf{v}_e\overleftrightarrow{\mathbf{P}}_e) - \overleftrightarrow{\mathbf{P}}_e\cdot\nabla\mathbf{v}_e - [\overleftrightarrow{\mathbf{P}}_e\cdot\nabla\mathbf{v}_e]^T - \frac{e}{m_e}(\overleftrightarrow{\mathbf{P}}_e\times\mathbf{B} + [\overleftrightarrow{\mathbf{P}}_e\times\mathbf{B}]^T) - \nabla\cdot\overleftrightarrow{\mathbf{Q}}, \tag{13}$$

where $\nabla\cdot\overleftrightarrow{\mathbf{Q}}$ denotes the divergence of the (triple) electron heat flux tensor. Figure 3 demonstrates that the overall evolution time scale τ is related to ion cyclotron time scales. Further investigations of the time evolution of the electron pressure tensor shows this to be true for the tensor components also. Therefore, we can assume

$$\tau \gg \Omega_e^{-1},\ L/v,$$

where L is a typical gradient scale length and v a typical electron flow velocity. With this assumption, Eq. (13) simplifies to

$$\nabla\cdot(\mathbf{v}_e\overleftrightarrow{\mathbf{P}}_e) + \overleftrightarrow{\mathbf{P}}_e\cdot\nabla\mathbf{v}_e + [\overleftrightarrow{\mathbf{P}}_e\cdot\nabla\mathbf{v}_e]^T + \frac{e}{m_e}(\overleftrightarrow{\mathbf{P}}_e\times\mathbf{B} + [\overleftrightarrow{\mathbf{P}}_e\times\mathbf{B}]^T) + \nabla\cdot\overleftrightarrow{\mathbf{Q}} = 0. \tag{14}$$

With the exception of the heat flux tensor, all terms in Eq. (14) scalelike the inverse electron cyclotron period or an inverse electron travel time. No immediate scaling is available for the heat flux contribution. Hesse *et al.*[8] ignored the heat flux contribution, which leads to the simplification of Eq. (14)

$$\nabla\cdot(\mathbf{v}_e\overleftrightarrow{\mathbf{P}}_e) + \overleftrightarrow{\mathbf{P}}_e\cdot\nabla\mathbf{v}_e + [\overleftrightarrow{\mathbf{P}}_e\cdot\nabla\mathbf{v}_e]^T + \frac{e}{m_e}(\overleftrightarrow{\mathbf{P}}_e\times\mathbf{B} + [\overleftrightarrow{\mathbf{P}}_e\times\mathbf{B}]^T) \approx 0. \tag{15}$$

The relevant pressure tensor components in Eq. (9) now follow from the same components of Eq. (15). For example, the x-y component of Eq. (15) becomes, after neglecting derivatives with respect to y,

$$\nabla\cdot(\mathbf{v}_e P_{xy}) + P_{xx}\partial_x v_y + P_{xz}\partial_z v_y + P_{xy}\partial_x v_x + P_{xy}\partial_x v_x + P_{yz}\partial_z v_x + \Omega_x P_{xz} + \Omega_z(P_{yy} - P_{xx}) - \Omega_y P_{yz} = 0. \tag{16}$$

Further assumptions are necessary. Near the reconnection site, the magnetic field is dominated by the guide field component. Specifically, we can assume that

$$B_y \gg B_x,\ B_z$$

in the region under investigation. Furthermore, it is reasonable to assume that electron distributions are nearly gyrotropic. This implies that the diagonal elements of the pressure tensor are much larger than the nondiagonal components, which are identical to the nongyrotropic components if the guide field dominates, or

$$P_{ii} \gg P_{ij}.$$

Under these assumptions, Eq. (16) and its y-z equivalent can be solved for the nongyrotropic pressure tensor components. In leading order these are

$$P_{xye} \approx -\frac{P_{zze}}{\Omega_e}\frac{\partial v_{ey}}{\partial z} + (P_{yye} - P_{zze})\frac{B_x}{B_y}, \tag{17a}$$

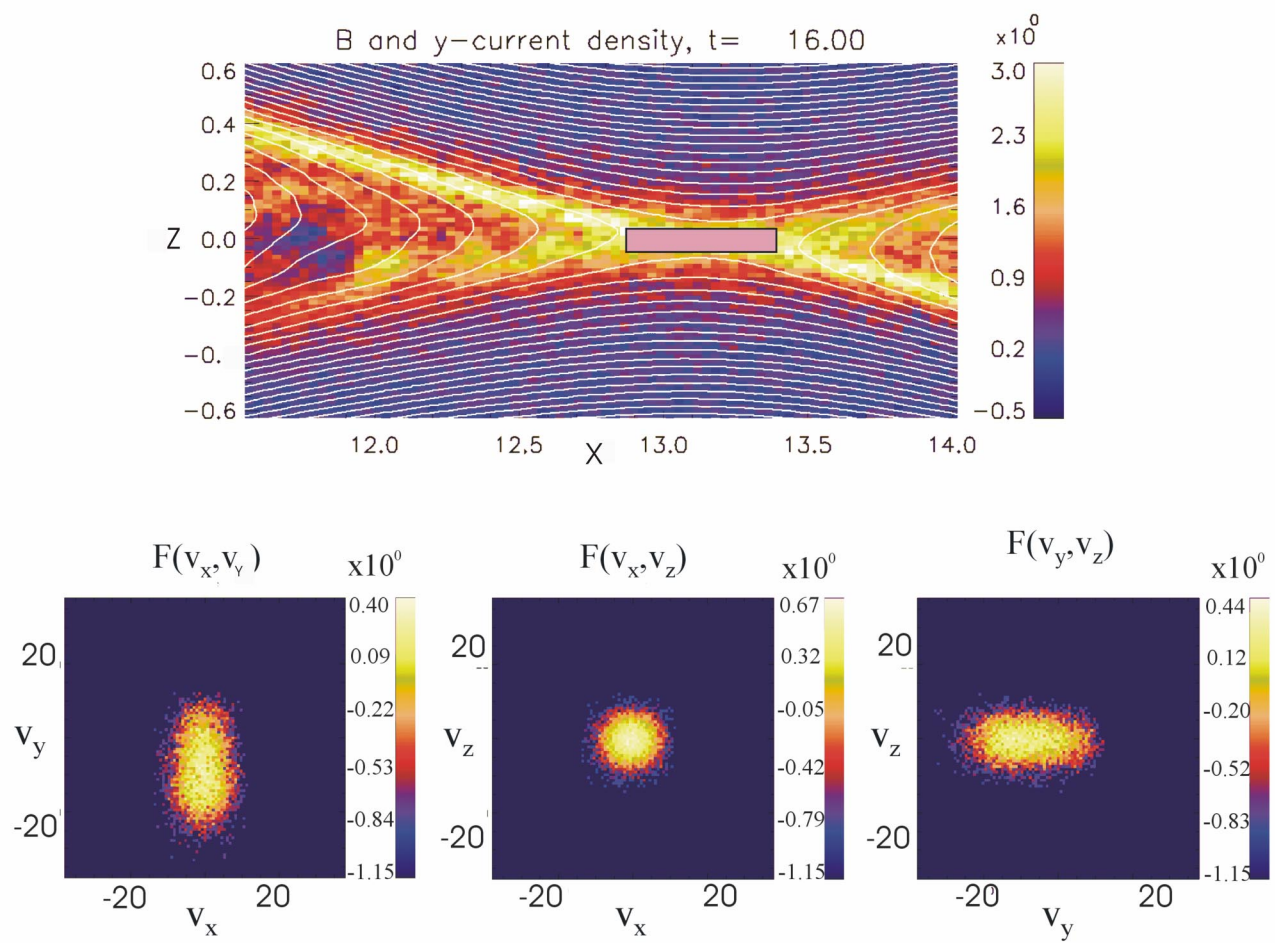

FIG. 5. (Color online). Reduced electron distribution functions near the center of the reconnection region. The top panel shows the location where particles were accumulated. The distribution is approximately gyrotropic.

$$P_{yze} \approx \frac{P_{xxe}}{\Omega_e}\frac{\partial v_{ey}}{\partial x} + (P_{yye} - P_{xxe})\frac{B_z}{B_y}. \tag{17b}$$

Here the first terms are anisotropy driver terms, whereas the second set of terms represent contributions primarily from the gyrotropic part of the pressure tensor. Equations (17) were first shown by Hesse *et al.*,[8] without a detailed presentation of the derivation. A comparison between actual simulation results and results from Eqs. (17) is shown in Fig. 7. Similar to the earlier display in Hesse *et al.*,[8] the panels show, at first glance, an apparent reasonable agreement between the direct simulation output and the approximation based on Eqs. (17). It is evident that the major contribution is from z derivatives of P_{yze}; in fact, the z derivative of P_{yze} is approximately independent of x.

However, a closer inspection of Fig. 7 reveals an important difference: While the particle data-derived values of P_{yze} (second panel) feature a clear gradient in the z direction at the reconnection location, at $\approx x=13.15$, this is not the case in the approximation, which is shown in the bottom panel. This deficiency would lead to a substantially reduced value of an approximate reconnection electric field, if that were calculated based on Eq. (17b). While P_{xye} appears to be remarkably well represented by Eq. (17a) (third panel), we thus find that Eq. (17b) does not represent the entire, dominant components of the pressure tensor component P_{yze} in the immediate vicinity of poloidal magnetic field null.

In order to investigate this discrepancy further, we solved Eq. (16) for P_{yze} without any further approximation. The result still did not reproduce the values of P_{yze} obtained directly from the simulation sufficiently well, even when adding time dependence back into the expression. Therefore, we are forced to conclude that neglecting the heat flux tensor appears not justified in the present calculation.

Adding the heat flux tensor back into Eq. (17b) leads to

$$P_{yze} \approx \frac{P_{xxe}}{\Omega_e}\frac{\partial v_{ey}}{\partial x} + (P_{yye} - P_{xxe})\frac{B_z}{B_y} + \frac{1}{\Omega_e}\left(\frac{\partial Q_{xxye}}{\partial x} + \frac{\partial Q_{xyze}}{\partial z}\right). \tag{18}$$

Derived from particle data without any further approximation, the heat flux tensor components Q_{xxye} and Q_{xyze}, as well as their derivatives are shown in Fig. 8. The lower panels demonstrate that the second, heat flux related, term in Eq. (18) is dominant in the immediate vicinity of the reconnection region. Therefore, Eq. (18) can be simplified as

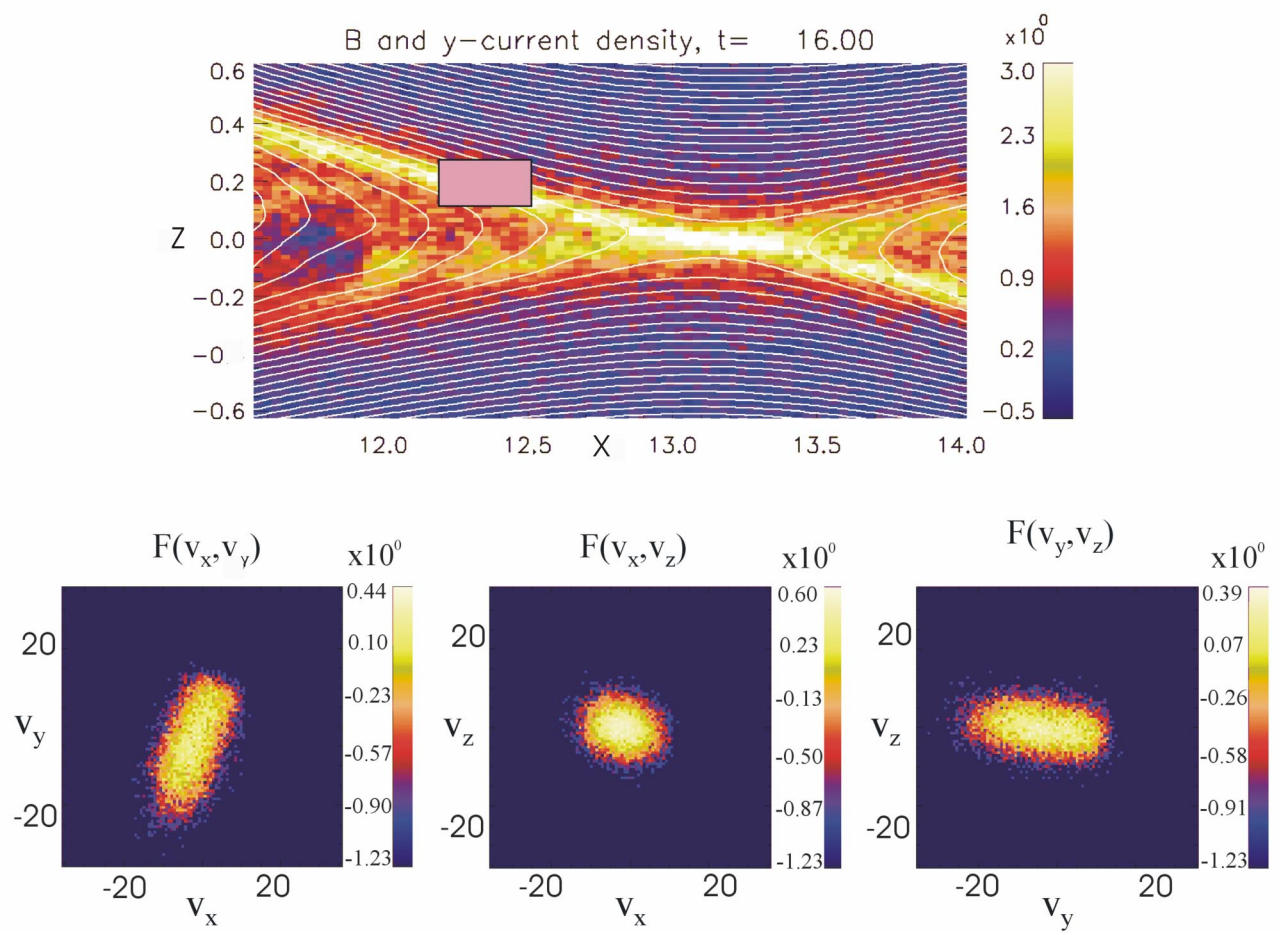

FIG. 6. (Color online). Reduced electron distribution functions away from the center of the reconnection region. The top panel shows the location where particles were accumulated. The distribution shows small deviations from gyrotropy.

$$P_{yze} \approx \frac{P_{xxe}}{\Omega_e}\frac{\partial v_{ey}}{\partial x} + (P_{yye} - P_{xxe})\frac{B_z}{B_y} + \frac{1}{\Omega_e}\frac{\partial Q_{xyze}}{\partial z}. \qquad (19)$$

The result of this approximation, depicted in Fig. 9, shows an excellent match with the direct determination of P_{yze} from the particle data. Thus we find that an appropriate approximation of the pressure nongyrotropy in the immediate vicinity of the neutral point of the poloidal magnetic field cannot be found without inclusion of a heat flux tensor component. This result is a major point of this paper.

Figure 10 shows that the pressure tensor varies on scales smaller than the electron inertial length. Instead, the electron Larmor radius in the guide magnetic field, approximately equal to $r_L = 0.03$, might provide the dominant scale length. Derivation of a scaling law of the reconnection process therefore requires the derivation of an analytic expression and of an evolution equation for the entire heat flux tensor. While Braginskii[25] developed suitable heat flux approximations for collisional plasmas, to our knowledge no such expression exists for collisionless systems. In the following section, we will therefore derive an approximate expression for Q_{xyze} and finally develop a reconnection scaling in Sec. VIII.

VII. EVOLUTION OF THE HEAT FLUX TENSOR AND APPROXIMATE REPRESENTATION OF Q_{xyze}

The heat flux tensor is defined in the electron center-of-mass system as

$$\vec{\mathbf{Q}} = m_s \int d^3u(\mathbf{u}-\mathbf{v})(\mathbf{u}-\mathbf{v})(\mathbf{u}-\mathbf{v})f_s. \qquad (20)$$

Here, f_s and m_s denote the distribution function and mass of plasma species s, $\mathbf{u}$ the phase space velocity, and $\mathbf{v}$ the bulk flow speed. An evolution equation for $\mathbf{Q}$ is obtained by multiplying the Vlasov equation by $\mathbf{uuu}$ and integrating over phase space. The result needs to be transformed into the center-of-mass frame of species s in order to derive an evolution equation for $\mathbf{Q}$. After lengthy algebra, one finds for the components of the heat flux tensor (index denoting species omitted for simplicity)

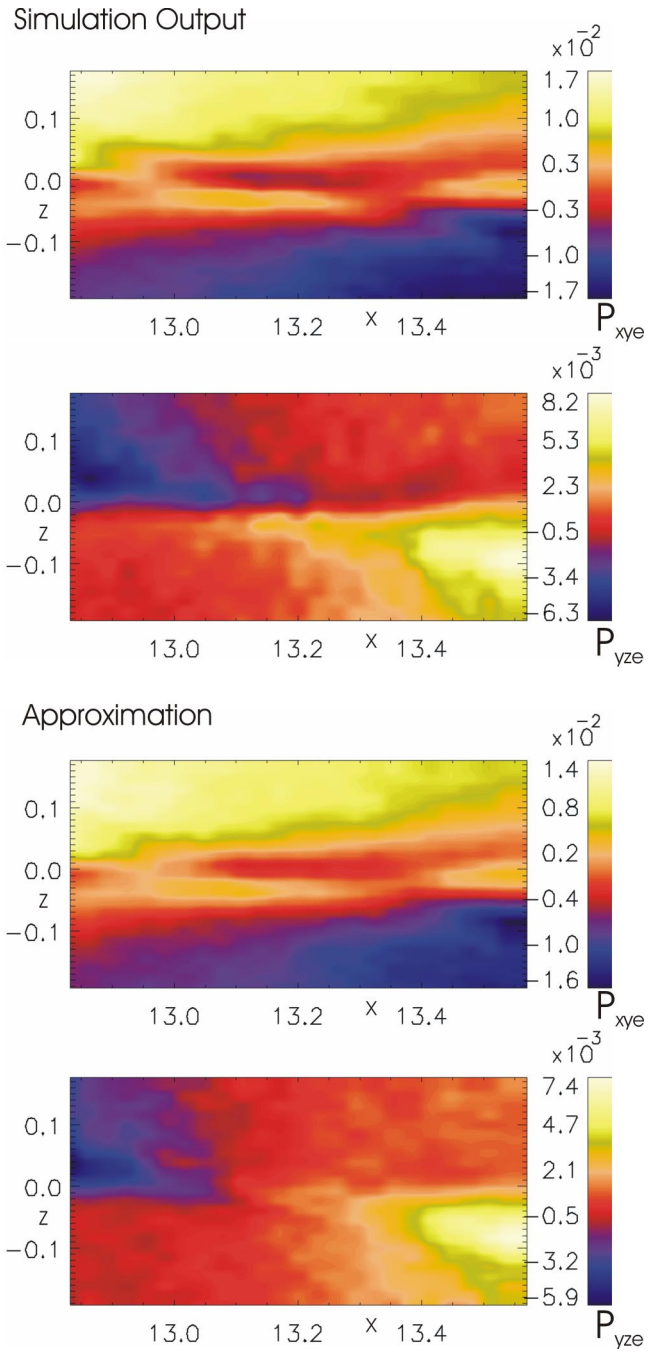

FIG. 7. (Color online). Electron pressure tensor components, derived directly from the particle information (top panels), or from the approximation (17) (bottom panels). While the x-y components match very well, the y-z components show a noticeable difference near $z=0$ and $x=13.15$.

$$\frac{\partial}{\partial t}Q_{ijk} + \sum_l \frac{\partial}{\partial x_l}(\Gamma_{ijkl} + P_{kl}v_iv_j + P_{il}v_jv_k + P_{jl}v_iv_k + Q_{ijk}v_l) + \sum_l Q_{lij}\frac{\partial}{\partial x_l}v_k + \sum_l Q_{ljk}\frac{\partial}{\partial x_l}v_i + \sum_l Q_{lik}\frac{\partial}{\partial x_l}v_j + \frac{e_s}{m_s}\sum_{r>s}\begin{bmatrix}(Q_{ijs}B_r - Q_{ijr}B_s)\varepsilon_{rsk}\\ +(Q_{iks}B_r - Q_{ikr}B_s)\varepsilon_{rsj}\\ +(Q_{jks}B_r - Q_{jkr}B_s)\varepsilon_{rsi}\end{bmatrix} = 0. \quad (21)$$

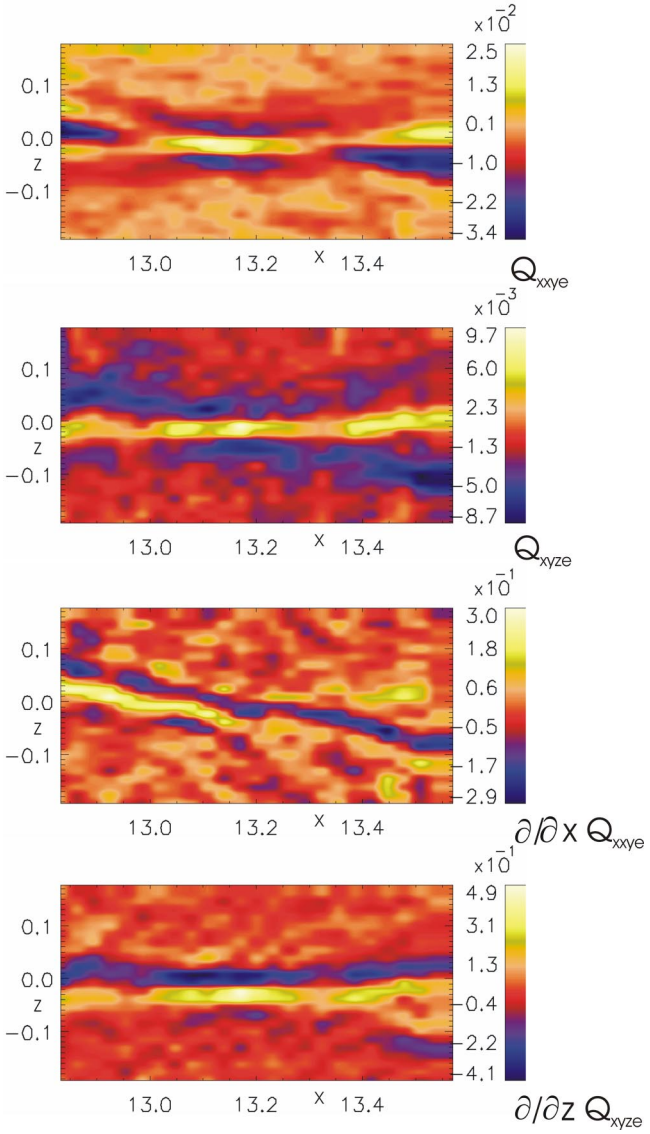

FIG. 8. (Color online). Relevant components of the heat flux triple-tensor (top panels) and their derivatives (bottom panels).

Here e_s denotes the charge of species s and ε_{ijk} is the usual, totally antisymmetric tensor. Equation (21) relates the time evolution of Q_{ijk} to lower order moments such as pressure and velocities, as well as to the fourth order tensor Γ_{ijkl}. The last term in Eq. (21) is a term, which represents the effects of particle cyclotron motion on the heat flux tensor in a similar way to the cyclotron term in Eq. (13). Clearly, Eq. (21) is invariant under change of order of indices, leading to a totally symmetric heat flux tensor.

Further progress toward a simple scaling relation requires simplifying assumptions. With similar arguments as in Sec. VI, we neglect time dependence. We also neglect the four tensor Γ_{ijkl}. We will see below that this neglect is acceptable. An expression for Q_{xyz} can now be obtained from the x,y,x-component of Eq. (21):

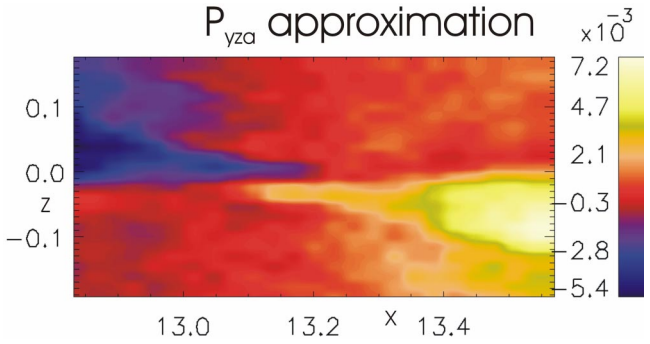

FIG. 9. (Color online). Approximation of the pressure tensor component P_{yze} that includes heat flux contributions. This approximation shows and excellent match with Fig. 7.

$$\sum_l \frac{\partial}{\partial x_l}(2P_{xl}v_xv_y + P_{yl}v_xv_x + Q_{xyx}v_l) + \sum_l Q_{lxy}\frac{\partial}{\partial x_l}v_x + \sum_l Q_{lyx}\frac{\partial}{\partial x_l}v_x + \sum_l Q_{lxx}\frac{\partial}{\partial x_l}v_y - \frac{e}{m_e}(2Q_{xyy}B_z - 2Q_{xyz}B_y + Q_{xxx}B_z - Q_{xxz}B_x) = 0. \quad (22)$$

Neglecting magnetic field components other than B_y, the convection term $\Sigma_l \partial/\partial x_l(Q_{xyx}v_l)$, and assuming $Q_{rst} < P_{rs}v_t$ (a reasonable assumption for a nearly gyrotropic plasma) near the reconnection region, reduces Eq. (22) to the simple expression

$$Q_{xyz} \approx -\frac{1}{\Omega_y}\left[\frac{\partial}{\partial x}(P_{xx}v_xv_y + 0.5P_{xy}v_x^2) + \frac{\partial}{\partial z}(P_{xz}v_xv_y + 0.5P_{yz}v_x^2)\right]. \quad (23)$$

In analogy to the derivation of Eq. (17), we recognize that the leading order term in Eq. (23) is

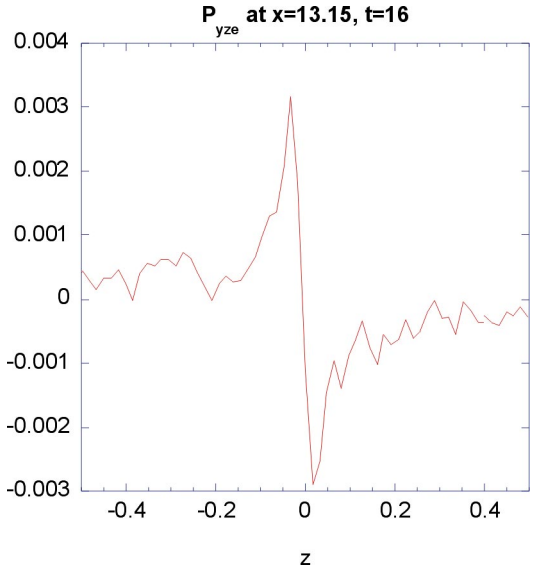

FIG. 10. (Color online). Plot of P_{yze} at $x=13.5$ and $t=16$. The figure demonstrates that the electron pressure tensor varies on scales smaller than the electron inertial length c/ω_{pe}, which is of a numerical value of approximately $c/\omega_{pe}=0.11$ in the location.

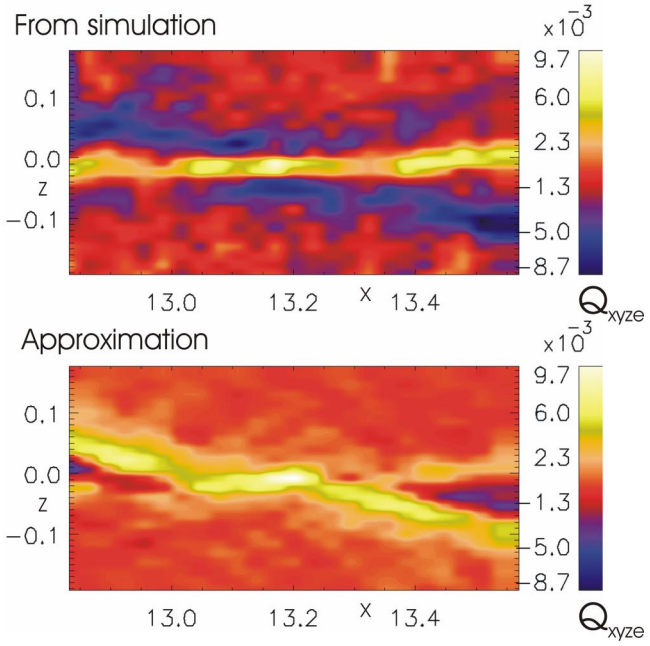

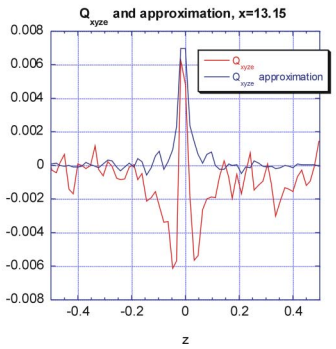

FIG. 11. (Color online). Approximate form of the heat flux tensor component Q_{xyze}. The figure shows that Q_{xyze} is reasonably well approximated in the very center of the current sheet. Our analysis indicates that further improvements in the approximation may be impossible without accounting for higher order moments of the distribution function.

$$Q_{xyz} \approx -\frac{1}{\Omega_y}\frac{\partial}{\partial x}(P_{xx}v_xv_y) \approx -\frac{P_{xx}v_y}{\Omega_y}\frac{\partial v_x}{\partial x} \quad (24)$$

for the relevant component of the electron heat flux tensor. Figure 11 shows a comparison between the heat flux tensor calculated directly from the simulation results and the approximation (24). The cut along the z direction shows that the central, positive feature in Q_{xyze} is reasonably well represented by the approximation (24) on electron Larmor scales ($r_L=0.03$ in this region). The negative values for larger z cannot be reproduced, even if all terms in Eq. (22) are included in the expansion. It remains highly likely that the four tensor Γ_{ijkl} needs to be included in order to account for all details of the heat flux tensor variations. Here, we restrict ourselves to an approximate reproduction of the main features of the heat flux tensor in the region of interest. In the following section, we will use this result to derive approximate scaling laws for the inner diffusion region.

VIII. APPROXIMATE SCALING OF THE DIFFUSION REGION DIMENSIONS

The analysis of Sec. IV showed that the inertia term in Eq. (9) constitutes a substantial contribution to the reconnection electric field. The reconnection region therefore has two transitions, the first, where the convection electric field becomes equal to the inertial electric field, at a scale L_1, and a second, L_2, where the inertial electric field is matched to the pressure tensor-derived electric field. L_1 is readily determined by the expansion:[1]

$$|E_{inertial}| \sim \frac{m_e}{e} v_z \frac{\partial v_y}{\partial x} \sim \frac{1}{{L_1}^2} \frac{B_0 v_z}{\mu_0} \frac{m_e}{e^2 n_e} = B_0 v_z \frac{c^2}{{\omega_{pe}}^2} \frac{1}{{L_1}^2}$$

$$= |E_{convection}| \frac{c^2}{{\omega_{pe}}^2} \frac{1}{{L_1}^2}. \tag{25}$$

The pressure electric field is derived from the first term of Eq. (9). With the addition of Eq. (24), the pressure tensor y-z component (20) becomes

$$P_{yze} \approx \frac{P_{xxe}}{\Omega_y} \frac{\partial v_{ey}}{\partial x} + (P_{yye} - P_{xxe}) \frac{B_z}{B_y} - \frac{1}{\Omega_y} \frac{\partial}{\partial z} \left(\frac{P_{xx} v_y}{\Omega_y} \frac{\partial v_x}{\partial x} \right), \tag{26}$$

where the last term dominates the reconnection electric field near the zero of the poloidal magnetic field. Ignoring lower order terms, and assuming a divergence-free electron velocity, the pressure electric field can be scaled as

$$|E_{Pressure}| \sim \frac{1}{n_e e} \frac{1}{\Omega_y} \frac{\partial^2}{\partial z^2} \left(\frac{P_{xx} v_y}{\Omega_y} \frac{\partial v_x}{\partial x} \right)$$

$$\sim \frac{1}{n_e e} \frac{1}{\Omega_y} \frac{\partial^2}{\partial z^2} \left(\frac{P_{xx} v_y}{\Omega_y} \frac{\partial v_z}{\partial z} \right)$$

$$\sim |E_{inertial}| \frac{1}{{L_2}^2} \frac{P_{xx}}{{\Omega_y}^2} \frac{1}{n_e m_e} = |E_{inertial}| \frac{{r_L}^2}{{L_2}^2}. \tag{27}$$

Equation (26) states that the transition from inertia-based to pressure-based dissipation occurs at a scale length equal to the electron Larmor radius in the guide magnetic field component. This is consistent with the electron pressure gradient scale inferred from Fig. 10.

Thus we find that there are two scale lengths associated with collisionless magnetic reconnection in the presence of moderate guide fields. The first, well-known scale is reached the inertial electric field equates the magnitude of the convection electric field. This scale length is the collisionless skin depth. For values of the electron $\beta = \mu_0 p_e / B^2$ of less than unity, the second transition occurs at a scale length of an electron Larmor radius in the guide magnetic field. The very small scales associated with the electron Larmor radius permit the heat flux to take on an unprecedented role in the electron dissipation process.

IX. SUMMARY AND CONCLUSIONS

In this paper, we presented an analysis of the electron diffusion region in collisionless magnetic reconnection, in the presence of a guide field of magnitude comparable to the reconnectiong magnetic field components. The analysis was based on a combination of numerical modeling and analytical theory. The analysis expands on a number of recent investigations of component merging. These studies were based on particle-in-cell simulations,[4–14] and hybrid and fluid modeling.[18,21,26,27]

During the analysis, we found that relatively extreme numerical resolution proved essential in order to resolve the small scales inherent in the electron diffusion region. Specifically, we found that resolving the electron Larmor radius in the guide field was necessary in order to resolve the gradient scale of the system in the inner diffusion region. In order to permit sufficient resolution and provide a large number of particles in each simulation cells, we therefore deliberately chose to study a translationally invariant model. The price to pay for this restriction is the omission of modes with finite k_y, such as those involved in Buneman instabilities and electron holes.[6] Therefore, our analysis cannot address the role such processes can play in the reconnection process. However, we did find a complete picture of how magnetic reconnection can operate, primarily by means of electron thermal inertia, even if a moderately sized guide magnetic field is present in the inner diffusion region.

The key question addressed by our investigation focused on the relative roles of electron bulk inertial processes and thermal inertial processes, the latter of which manifest themselves in nongyrotropic electron pressure tensors.[7] When studying the inertial contribution to the reconnection electric field, we found that there is indeed a finite contribution from bulk inertia, inside of a collisionless skin depth scale length. This result is consistent with the recent investigation by Pritchett and Coroniti.[19] In addition, however, we also found further contributions of the electron pressure tensor inside a smaller scale length, where, in fact, the inertial contribution dropped to zero. Here, nongyrotropic pressures were indeed seen, with gradients sufficient to support the reconnection electric field in the very center of the reconnection region.

Studying electron distribution functions in the diffusion region, we found small deviations from gyrotropic distributions, consistent with the presence of nongyrotropic pressures. We used this feature to derive an approximate expression for the electron pressure tensor in the neighborhood of the null in the poloidal magnetic field. The results were identical to those derived by Hesse *et al.*[8] When comparing the pressure tensor so derived with values derived directly from the simulation model, we discovered an unexpected and significant difference near the null of the reconnecting field. This difference proved sufficient to invalidate the previous electron pressure tensor approximation.

Reintroduction of additional terms into the expression for the pressure tensor proved ineffective, as long as the divergence of the heat flux tensor was not included. We therefore calculated the third moments from the particle data. The results showed that inclusion of the heat flux is necessary to reproduce the electron pressure tensor in the reconnection region. This is one of the main results of the present study. In pursuit of the goal to scale the electron pressure and reconnection electric field, we therefore derived the evolu-

tion equation of the heat flux three tensor. Assuming the heat flux tensor components are small compared to products between pressure and velocity, we could reduce this equation to an approximation for the specific heat flux tensor element, which is relevant to the pressure tensor evolution. We showed that the approximation accounts for the heat flux in the inner region reasonably well, whereas a complete description requires accounting for the next, four tensor in the heat flux evolution equation.

Based on our approximation, we were able to derive the length scales relevant to the reconnection process. We found that the inertial electric field supercedes the convection electric field as the main contributor to the reconnection electric field at a distance of approximately a collisionless skin depth from the center of the electron current layer. A further transition occurs at a distance of approximately an electron Larmor radius from the current layer center. At this distance, the inertial effects disappear and electron pressure effects (thermal inertial effects) become dominant. This transition remedies the logarithmic singularity in the electron flow velocity, which would otherwise be required to balance the reconnection electric field.

We remark that the transition to electron inertial effects occurs first because the electron Larmor radius in the guide field is smaller than the electron skin depth. This is the case if the electron $\beta = \mu_0 p_e / B^2$ is smaller than unity. For $\beta = \mu_0 p_e / B^2$ greater than unity, it is conceivable that inertial electric fields may be overall less important than in the present study. This topic, however, is the subject of a future investigation.

While the analysis here has been developed with electrons in mind, it is clear that similar if not identical arguments and theoretical approximation can be derived for ions also. Particle-in-cell modeling of proton-antiproton plasmas show very similar effects in the presence of a guide field, albeit on ion scales. The discussion of ion behavior, however, is outside of the scope of this paper and will be the subject of a future publication.

Finally, we emphasize the serious demands that the requirement to resolve the electron Larmor radius imposes on numerical models, including the one used in this investigation. This concern will become more severe for even stronger guide fields than employed here. We hope, however, that the combination of numerical modeling and theoretical analyses presented in this paper help to shed light on the way reconnection operates in the presence of a guide magnetic field.

ACKNOWLEDGMENTS

This research was supported by NASA's Sun-Earth Connection Theory Program (SECTP). We appreciate stimulating discussions with K. Schindler and J. Drake.

[1] V. M. Vasyliunas, Rev. Geophys. Space Phys. **13**, 303 (1975).
[2] K. Schindler, M. Hesse, and J. Birn, Astrophys. J. **380**, 293 (1991).
[3] M. Hesse and D. Winske, J. Geophys. Res. **99**, 11177 (1994).
[4] J. Birn, J. F. Drake, M. A. Shay *et al.*, J. Geophys. Res., [Space Phys.] **106**, 3715 (2001).
[5] J. F. Drake and M. E. Mandt, Geophys. Res. Lett. **73**, 1251 (1994).
[6] J. F. Drake, M. Swisdak, C. Cattell, M. A. Shay, B. N. Rogers, and A. Zeiler, Science **299**, 873 (2003).
[7] M. Hesse, K. Schindler, J. Birn, and M. Kuznetsova, Phys. Plasmas **6**, 1781 (1999).
[8] M. Hesse, M. Kuznetsova, and M. Hoshino, Geophys. Res. Lett. **29**, 1563 (2002).
[9] H. Karimabadi, D. Krauss-Varban, and N. Omidi, J. Geophys. Res., [Space Phys.] **104**, 12,313 (1999).
[10] P. L. Pritchett, J. Geophys. Res., [Space Phys.] **106**, 3783 (2001).
[11] P. L. Pritchett, J. Geophys. Res., [Space Phys.] **106**, 25961 (2001).
[12] P. Ricci, G. Lapenta, and J. U. Brackbill, Geophys. Res. Lett. **29**, 2088 (2002).
[13] B. N. Rogers, R. E. Denton, and J. F. Drake, J. Geophys. Res., [Space Phys.] **108**, 1111 (2003).
[14] A. Zeiler, D. Biskamp, J. F. Drake, B. N. Rogers, M. A. Shay, and M. Scholer, J. Geophys. Res., [Space Phys.] **107**, 1230 (2002).
[15] L. R. Lyons and D. C. Pridmore-Brown, J. Geophys. Res., [Space Phys.] **95**, 20903 (1990).
[16] J. D. Scudder, F. S. Mozer, N. C. Maynard, and C. T. Russell, J. Geophys. Res., [Space Phys.] **107**, 1294 (2002).
[17] R. Horiuchi and T. Sato, Phys. Plasmas **1**, 3587 (1994).
[18] M. M. Kuznetsova, M. Hesse, and D. Winske, J. Geophys. Res., [Space Phys.] **103**, 199 (1998).
[19] P. L. Pritchett and F. V. Coroniti, J. Geophys. Res., [Space Phys.] **109**, A0122O (2004).
[20] D. Biskamp and K. Schindler, Plasma Phys. Controlled Fusion **13**, 1013 (1971).
[21] D. Krauss-Varban, H. Karimabadi, and N. Omidi, Geophys. Res. Lett. **26**, 1235 (1999).
[22] M. Swisdak, B. N. Rogers, J. F. Drake, and M. A. Shay, J. Geophys. Res., [Space Phys.] **108**, 1218 (2003).
[23] E. G. Harris, Nuovo Cimento **23**, 115 (1962).
[24] M. Hesse and D. Winske, J. Geophys. Res., [Space Phys.] **99**, 11177 (1994).
[25] S. I. Braginskii, *Transport Processes in a Plasma*, Reviews of Plasma Physics Vol. 1, (Consultants Bureau, New York, 1965), p. 205.
[26] M. Kuznetsova, M. Hesse, and D. Winske, J. Geophys. Res., [Space Phys.] **106**, 3799 (2001).
[27] M. A. Shay, J. F. Drake, M. Swisdak, W. Dorland, and B. N. Rogers, Geophys. Res. Lett. **30**, 1345 (2003).